Supporting Information

CVD synthesis and optical study of bandgap-tunable Sn-doped monolayer molybdenum disulfide

Yuxin Zhang[1,2], Zhengbo Zhong[2], Yuhao Mi[2], Jiawei Duan[2], Tianhui Ren[2,*], Sheng Han[1,*], Zhipeng Li[2,*]

1. School of Chemical and Environmental Engineering, Shanghai Institute of Technology, Shanghai, 201418, China
2. School of Chemistry and Chemical Engineering, Shanghai Jiao Tong University, Shanghai, 200240, China.

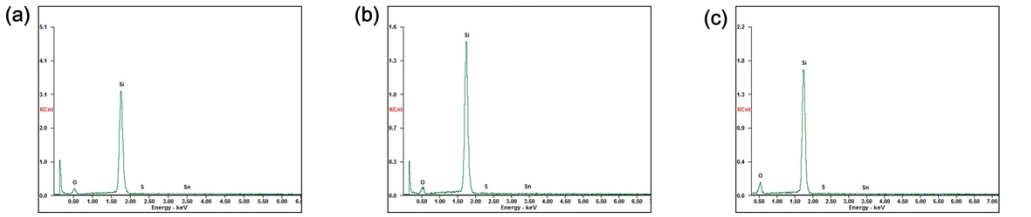

Element	Wt%	At%
OK	05.39	09.18
SiK	93.10	90.32
SK	00.25	00.21
SnL	01.26	00.29

Element	Wt%	At%
OK	04.28	07.36
SiK	94.21	92.18
SK	00.19	00.16
SnL	01.32	00.31

Element	Wt%	At%
OK	08.42	14.08
SiK	89.47	85.20
SK	00.39	00.33
SnL	01.72	00.39

Figure S1. EDS spectrum of Sn-doped MoS_2.(a) 3 wt.% Sn-MoS_2. (b) 6 wt.% Sn-doped MoS_2. (c) 12 wt.% Sn-doped MoS_2.

because the detection depth of the EDS is around 1~3 μm and the monolayer of MoS_2 is ~0.7 nm, the results show an extremely weak signal for the components of Sn-doped MoS_2, which is dominant by the Si and O from the substrate. It is better to conduct the TEM-EDS to extract the component information, and we are still trying to develop a feasible transfer way for the sample preparation for TEM measurement. Even though, our EDS results still show a gradient increase with the increase in the proportion of the precursor (the atomic percentage of Sn rises from 0.29 At% to 0.39 At%).

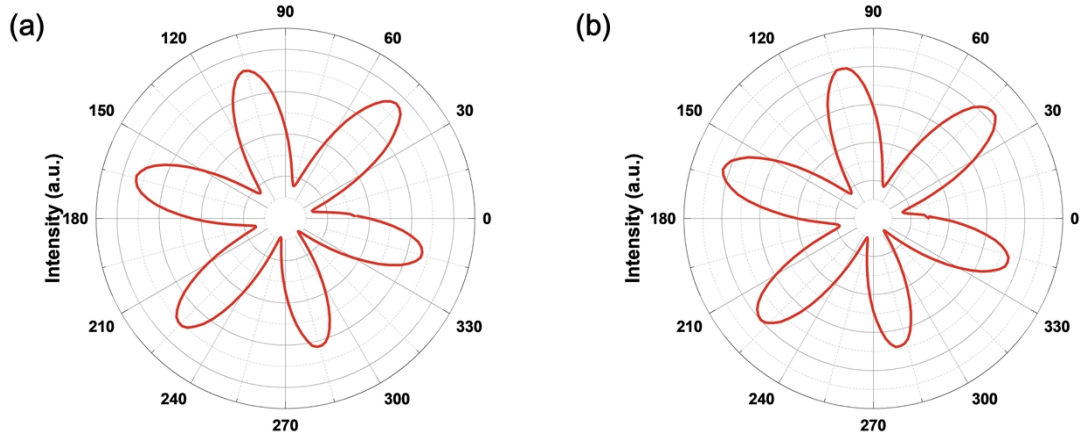

Figure S2. (a) Polar plots of parallel components of second harmonic generations (SHG) intensity of 3 wt.% Sn-doped MoS_2. (b) Polar plots of parallel components of second harmonic generations (SHG) intensity of 12 wt.% Sn-doped MoS_2.

We have performed second harmonic generation (SHG) intensity measurements on 3 wt.% Sn-doped MoS_2 and 12 wt.% Sn-doped MoS_2 and found that the doping concentration does not have a significant effect on the second harmonic triple symmetry of MoS_2, which both exhibit good symmetry. It indicates that Sn doping did not break the lattice symmetry of MoS_2.

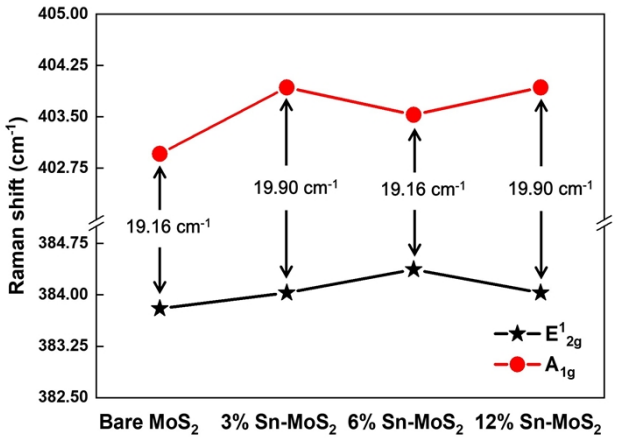

Figure S3. Modes of E^1_{2g} and A_{1g} Raman vibrations in (Sn-) MoS_2 with different doping concentrations.

The Raman spectra of MoS_2 exhibit characteristic blue shifts in both E^1_{2g} and A_{1g} phonon modes after Sn doping, indicating the introduction of tensile stress within the monolayer structure. Specifically, the 3 wt.% and 12 wt.% doped samples show consistent shifts of +0.23 cm^{-1} (E^1_{2g}) and +0.97 cm^{-1} (A_{1g}), while the 6 wt.% doped sample demonstrates equal blue shifts of +0.57 cm^{-1} for both modes. Notably, the A_{1g}-E^1_{2g} peak separation remains characteristic of monolayer MoS_2 (19.16 cm^{-1} for undoped and 6 wt.% doped, 19.90 cm^{-1} for 3 wt.% and 12 wt.% doped), confirming preserved monolayer integrity.

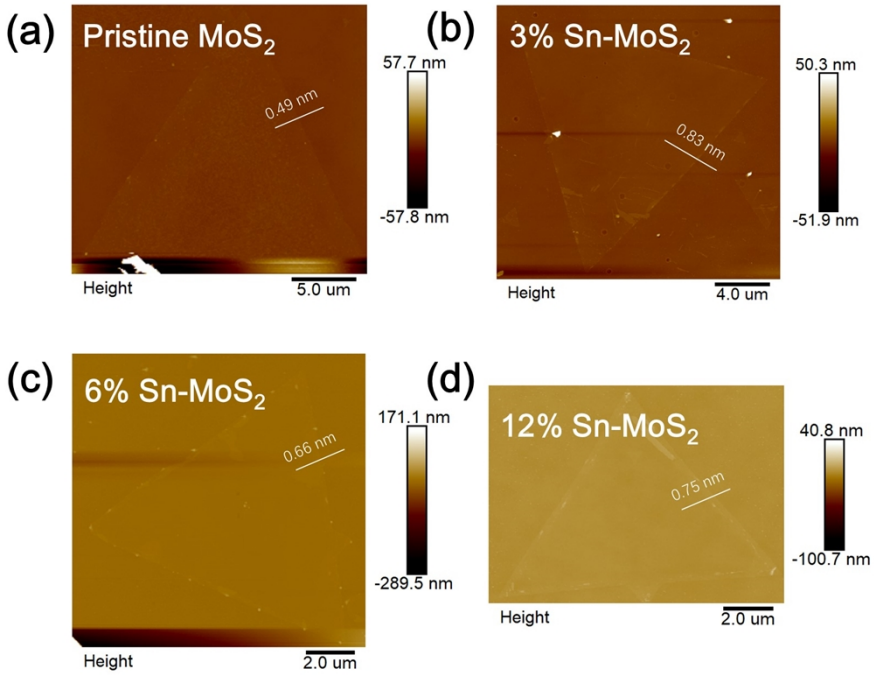

Figure S4. AFM images of pristine, 3 wt.%, 6 wt.%, and 12 wt.% Sn-doped MoS_2.

AFM measurements (Fig.S4) clearly demonstrate that both pristine and Sn-doped

MoS_2 maintain monolayer characteristics, with measured thicknesses of 0.49 nm (pristine), 0.83 nm (3 wt.% Sn), 0.66 nm (6 wt.% Sn), and 0.75 nm (12 wt.% Sn).

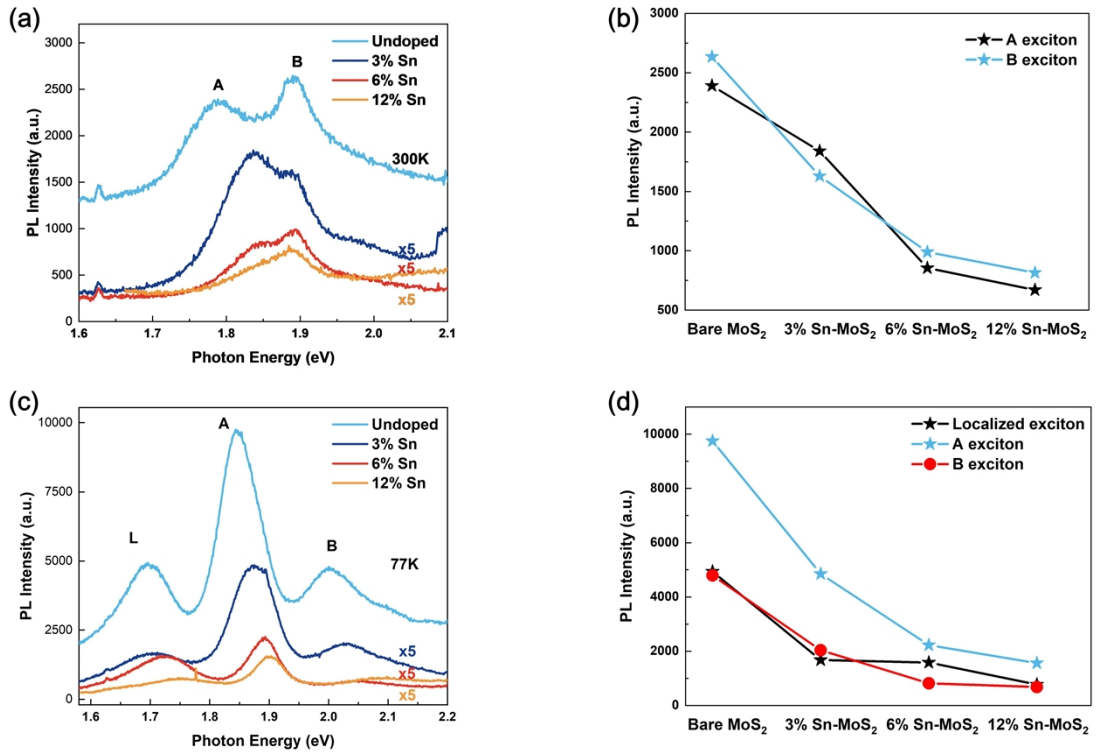

Figure S5. (a) Intensity variation of PL spectra with doping concentration at room temperature. (100 μW) (b) The comparison of A exciton and B exciton of the as-prepared samples at room temperature in PL spectrum. (c) Intensity variation of PL spectra with doping concentration at low temperature (77 K). (200 μW) (d) The comparison of localized exciton, A exciton and B exciton of the as-prepared samples at low temperature (77K) in PL spectrum.

The PL intensity of MoS_2 at room temperature and 77 K progressively decreases with increasing Sn doping concentration, in which both A and B excitons show a linear decline. In particular, at room temperature, the trend of decreasing PL intensity was significant as the doping concentration increased from 3 wt.% to 6 wt.%. At 77 K, the decreasing trend of PL intensity was evident at a doping concentration of 3 wt.%.

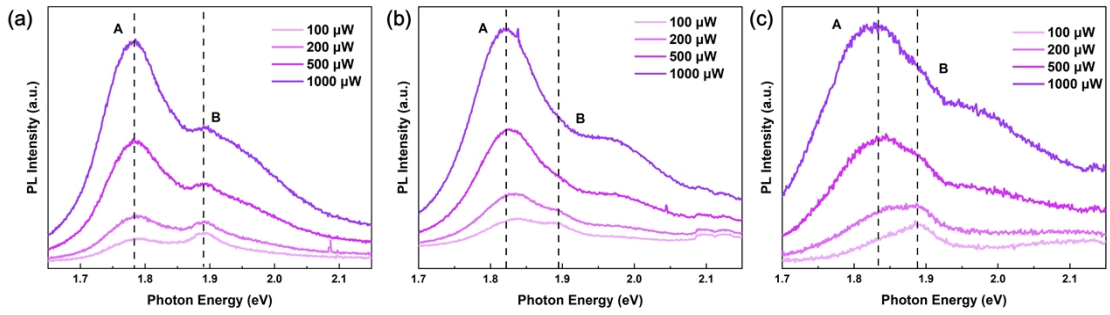

Figure S6. (a) PL spectrum of Pristine MoS_2 with 100, 200, 500 and 1000 μW power at room temperature, respectively. (b) PL spectrum of 3 wt.% Sn-doped MoS_2 with 100, 200,

500 and 1000 μW power at room temperature, respectively. (c) PL spectrum of 12 wt.% Sn-doped MoS_2 with 100, 200, 500 and 1000 μW power at room temperature, respectively.

We conducted PL with power testing of Pristine MoS_2, 3 wt.% Sn-doped MoS_2 and 12 wt.% Sn-doped MoS_2 at room temperature, and found that the A exciton and B exciton of MoS_2 were gradually enhanced as the power was gradually increased from 100 μW to 1000 μW. In particular, the A exciton and B exciton peak shapes are obvious when the power reaches 500 μW.

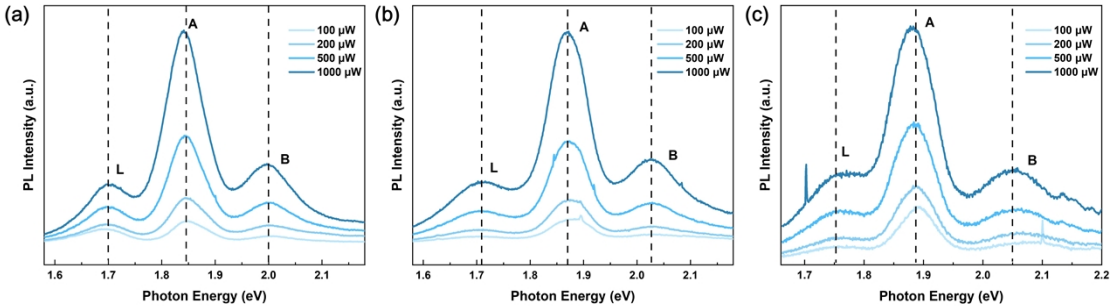

Figure S7. (a) PL spectrum of undoped MoS_2 with 100, 200, 500 and 1000 μW power at low temperature (77 K), respectively. (b) PL spectrum of 3 wt.% Sn-doped MoS_2 with 100, 200, 500 and 1000 μW power at low temperature (77 K), respectively. (c) PL spectrum of 12 wt.% Sn-doped MoS_2 with 100, 200, 500 and 1000 μW power at low temperature (77 K), respectively.

We conducted PL tests of Pristine MoS_2, 3 wt.% Sn-doped MoS_2 and 12 wt.% Sn-doped MoS_2 with power at 77 K. We found that the A exciton, B exciton and Localized exciton of MoS_2 are gradually enhanced as the power is raised from 100 μW to 1000 μW progressively. At 100 μW, the A exciton, B exciton and Localized exciton peaks are obvious.

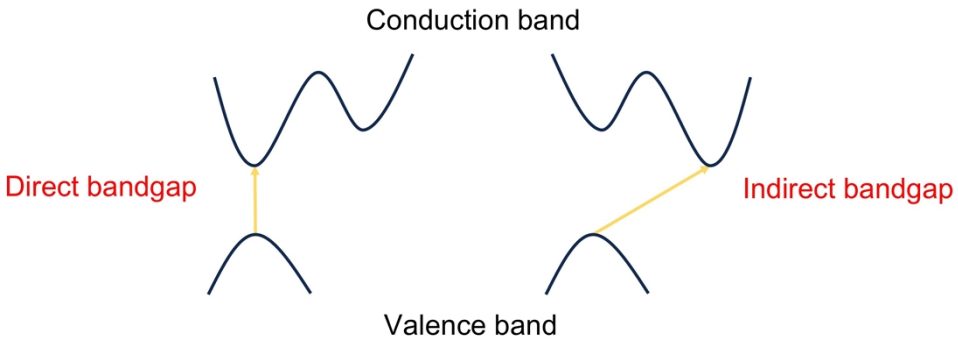

Figure S8. Possible band structure evolution of molybdenum disulfide before and after Sn-doping.

Sn doping has an important effect on the MoS_2 energy band structure, we hypothesize that this change may originate from the Sn-doping-induced energy band structure transition, i.e., MoS_2 is transformed from a pristine direct bandgap semiconductor to a semi-indirect bandgap semiconductor. This transition can explain the weakening of the PL signal because the radiative complexation probability of electron-hole pairs is significantly reduced in indirect bandgap materials. At the same time, the shift in the bandgap type leads to an increase in the bandgap energy, which coincides with the observed PL blue shift phenomenon.

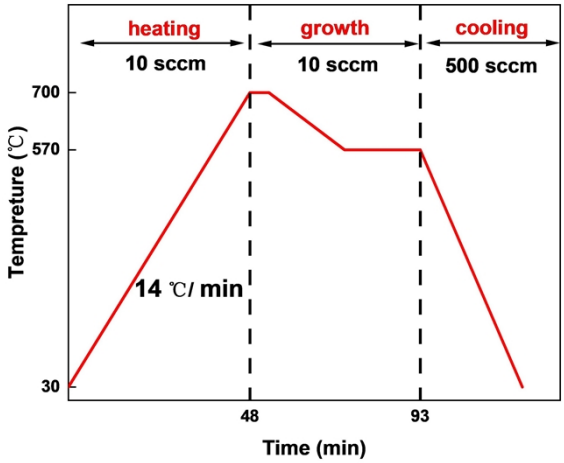

Figure S9. The temperature program of the one-step CVD process for pristine MoS_2 and Sn-doped MoS_2.

Here, the heating zone was heated from 30℃ to 700℃ in 48 min and then kept for 5 min. Next, the temperature reaches 570℃ in 13 minutes and is held for 20 minutes. Keep the N_2 flow rate at 10 sccm for heating and growing, and set the carrier gas flow rate to 500 sccm for rapid cooling.

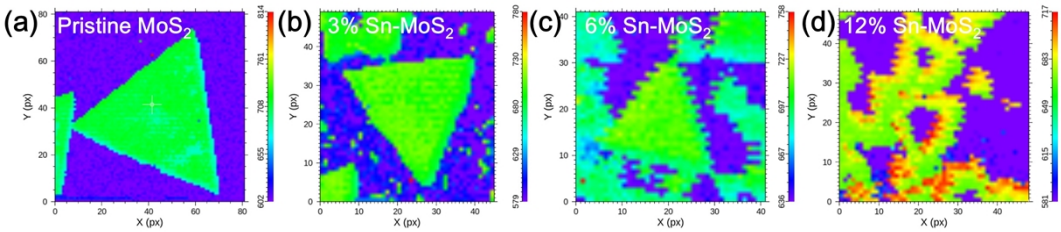

Figure S10. PL mapping wavelength corresponding to pristine MoS_2, 3 wt.%, 6 wt.%, and 12 wt.% Sn-doped MoS_2.

PL emission peaks are systematically blue-shifted from ~720 nm (pristine MoS_2) to 700 nm (3 wt.% Sn), 697 nm (6 wt.% Sn), and finally to 650 nm (12 wt.% Sn), demonstrating a doping-dependent bandgap widening. This trend can be attributed to the compressive strain resulting from the substitution of Mo sites by larger Sn ions, which increases the bandgap of the monolayer MoS_2.

Figure S11. Optical images of MoS_2 under different growth temperatures.

Through a series of experiments, we found that at lower temperatures (500~600 °C), MoS_2 has inferior crystallization quality and more defects, while at higher temperatures (above 800 °C), it is likely to form multilayers or thick film structures, which affects the film quality. At 700 °C, MoS_2 achieves the optimal crystallization quality, film uniformity, and larger grain sizes as well as lower defect densities.